Correlation between thermal deformation and microcracking in concrete during cryogenic cooling

Reginald B. Kogbara[1*], Srinath R. Iyengar[1], Zachary C. Grasley[2], Syeda Rahman[2], Eyad A. Masad[1,2], Dan G. Zollinger[2]

[1]Mechanical Engineering Program, Texas A&M University at Qatar, P.O. Box 23874, Education City, Doha, Qatar.

[2]Zachry Department of Civil Engineering, Texas A&M University, College Station, TX 77843, USA.

* Corresponding author email: regkogbara@cantab.net

Abstract

Thermal deformation behavior of concrete mixtures from limestone and trap rock aggregates has been related to microcracking during cryogenic cooling. The study was aimed at comparing the suitability of the concretes for direct containment of liquefied natural gas (LNG). The results showed strong correlation between the thermal strain rate and the acoustic emission (AE) cumulative hits rate in the concretes. The closeness of the average thermal expansion coefficient of the trap rock mixture over the ambient to cryogenic temperature range to that of 9% Ni or carbon-steel, and its lower cumulative energy emission corroborates previous observations on its porosity, permeability and microstructural behavior. These likely make it more suitable for direct LNG containment.

Keywords: Acoustic emission; coefficient of thermal expansion; limestone aggregate; strain gage; trap rock aggregate.

This is an author-created version: regkogbara@cantab.net (RB Kogbara). A definitive version was subsequently published at http://dx.doi.org/10.1016/j.ndteint.2015.09.002 in *NDT&E International*, Volume 77, pp 1 – 10 (2016). The final publication is available at www.sciencedirect.com.

Correlation between thermal deformation and microcracking in concrete during cryogenic cooling

Reginald B. Kogbara[1*], Srinath R. Iyengar[1], Zachary C. Grasley[2], Syeda Rahman[2], Eyad A. Masad[1,2], Dan G. Zollinger[2]

[1]Mechanical Engineering Program, Texas A&M University at Qatar,
P.O. Box 23874, Education City, Doha, Qatar.
[2]Zachry Department of Civil Engineering, Texas A&M University,
College Station, TX 77843, USA.

Abstract

Thermal deformation behavior of concrete mixtures from limestone and trap rock aggregates has been related to microcracking during cryogenic cooling. The study was aimed at comparing the suitability of the concretes for direct containment of liquefied natural gas (LNG). The results showed strong correlation between the thermal strain rate and the acoustic emission (AE) cumulative hits rate in the concretes. The closeness of the average thermal expansion coefficient of the trap rock mixture over the ambient to cryogenic temperature range to that of 9% Ni or carbon-steel, and its lower cumulative energy emission corroborates previous observations on its porosity, permeability and microstructural behavior. These likely make it more suitable for direct LNG containment.

Keywords: Acoustic emission; coefficient of thermal expansion; limestone aggregate; strain gage; trap rock aggregate.

[*] Corresponding author email: regkogbara@cantab.net. Tel: +974 4423 0289.

1. Introduction

Traditional liquefied natural gas (LNG) storage tanks utilize 9% Ni steel for the primary containment tank as it has greater ductility at cryogenic temperatures (i.e. ≤ -165°C) compared to normal carbon-steel. However, 9% Ni steel is becoming increasingly expensive. Literature review shows that concrete properties generally improve at cryogenic temperatures [1, 2]. Utilizing concrete for conventional 160,000 m^3 capacity LNG tanks, which costs US$130 million or more, would lead to at least 10 – 15% cost savings [3]. The development of the standard on concrete structures for containment of refrigerated liquefied gases, ACI 376-11 [4] may increase the impetus for tank designs utilizing concrete for primary LNG containment. However, concrete behavior at cryogenic temperatures is not fully elucidated. Thus, this work seeks to study damage evolution in concrete during cooling due to stresses associated with coefficient of thermal expansion (CTE) mismatch between concrete components.

Studies have shown that concrete cured at 20°C and 65% relative humidity (RH) exhibits an almost linear strain behavior when cooled below 0°C. In contrast, water-saturated (wet cured) concrete exhibits a three-stage behavior with expansion between -20°C and -70°C preceded and followed by contraction [1, 2, 5, 6]. Similarly, there is a sudden decrease in the CTE between 0°C and -75°C depending on the moisture content. A critical RH of 86% has been identified, with the CTE of concrete stored below this value being governed by aggregate type and those stored above 86% RH governed by moisture content [1, 7]. Majority of previous studies on damage in cryogenic concrete focused on thermal strains. Thus, there is a dearth of information on measures of concrete damage like acoustic emission (AE), microstructure examination, and changes in porosity and permeability due to internal cracking. These have been the subject of recent related studies [8, 9]. Thermally generated stresses could induce AE through microscopic deformation. AE signals are transient elastic waves emitted as a consequence of crack initiation and propagation or friction activation in existing cracks. Therefore, AE is a valuable tool for damage monitoring as it is capable of identifying failure mechanisms [10, 11].

In the design of a concrete LNG tank, which is subjected to large temperature swings, the stresses and strains due to differences in CTE between concrete and steel must be considered. For instance, a drop of about 188°C (338°F) during cooling of the tank wall at ~1°C/hour is reported to cause contraction such that the composite concrete wall of a 160,000 m^3 capacity tank moves approximately 64 mm inward. The 9% Ni steel tank bottom, which is attached to the tank wall at its base, also contracts. Thus, the more similar the CTEs of the tank wall and bottom materials, the less tension is developed in the tank bottom plating and this must be considered in design [12]. The CTE of carbon-steel and 9% Ni steel are similar over the ambient to cryogenic temperature range [12]. *ArcelorMittal* reports a mean CTE value of 8.8 µstrain/°C for the -196 °C to 21°C range, and 9.9 µstrain/°C for the -129°C to 21°C range, for 9% Ni steel [13]. In contrast, the CTE of concrete could vary from 7 – 13 µstrain/°C at ambient temperature and may even decrease to negative values followed by subsequent increase during cryogenic cooling [2]. The extent of the variation depends mainly on the aggregate type, with significant influence from the degree of water saturation of the concrete. Hence, it was recommended that aggregates with a low CTE that is compatible with the cement matrix and a water/cement (w/c) ratio $\leq$ 0.45 be used in concrete LNG tanks [4].

In light of the above, this work sought to evaluate and compare the suitability of two concrete mixtures produced with limestone and trap rock aggregates for use in direct LNG containment. The mixtures were shortlisted after testing different concrete mixtures subjected to cryogenic cooling for changes in porosity, mean pore size and internal microstructure using different non-destructive techniques, and water permeability [8, 9]. The objective of this research was to investigate whether AE parameters such as cumulative hits and energy rates could provide a good indication of the strain rate in concrete during cryogenic cooling. It also investigated the existence of a relationship between the change in strain per unit temperature drop and cumulative hits and energy per unit temperature. The cumulative hits and energy per unit temperature are AE emission rate per temperature decrement parameters [14], which refer to the cumulative hits and cumulative energy build-up within a given temperature range during cooling. A very large increment in cumulative energy and hits per unit temperature change in a given interval could be related physically to a high damage growth rate in the concrete during cooling. Both parameters are introduced here to evaluate how they vary with the thermal strain within selected temperature ranges that are crucial during water freezing and frost damage in concrete [1]. The research also sought to compare the closeness of the CTE behavior of the concrete mixtures to that of 9% Ni or carbon-steel over the ambient to cryogenic temperature range.

2. Experimental methodology

2.1 Production of concrete specimens

The concrete mixtures were prepared with river sand as fine aggregate using limestone and trap rock as coarse aggregates. The aggregates were obtained from quarries in Texas, USA. The physical properties and mineralogical composition of the aggregates have been documented in a related publication [8]. The maximum coarse aggregate size employed was 19 mm. Type I portland cement was used for casting of the 75 mm diameter and 150 mm long cylindrical concrete specimens. The w/c ratio was 0.42. Table 1 shows key details of the mixture design used. The 28-day compressive strength values [15] correspond to the minimum specified for concrete for refrigerated liquefied gases when containing liquids (34.5 MPa) in the ACI 376 code [4]. The specimens were cured under water until preparation for testing.

2.2 Specimen preparation for strain gage installation

After 55 days of water curing, the concrete specimens were air-dried for about 2 hours in the laboratory at 20°C and 50% RH. The specimens were then cleaned to remove any laitance or other soiling from the gage installation area. Thereafter, grade 120 abrasive papers were used to abrade an area for strain gage installation. The specimens were abraded continuously for 8 - 10 minutes, and then thoroughly cleaned with tissue paper until the final tissue used was stain-free. This step was repeated twice and the entire abrading and cleaning process lasted about 25 – 30 minutes. The result was a polished surface, which exposed the smaller aggregates of the concrete. It should be noted that this step is quite critical to correct strain measurement by the bonded gage, especially during soaking at a given temperature. Preliminary testing showed that inadequate abrading of the concrete specimen leads to delayed thermal behavior where the thermal output decreases continuously, as the chamber temperature is kept constant, irrespective of the temperature in question.

The abraded surface of the gage installation area was precoated with M-bond 43-B adhesive / coating material (*Vishay Precision Group - VPG*, USA). The coating acts as a barrier against any dampness that is exuded from the surface of the concrete, thereby preventing absorption of moisture by the underside of the strain gage. Thereafter, a thin layer of cyanoacrylate (CN) adhesive (*TML*, Japan) was applied uniformly over the entire back of the strain gage. The gage was then firmly bonded to the concrete surface. A layer of K-1 coating material (special rubber for moisture proofing, *TML*, Japan) was then applied over the gage installation area. The whole assembly was then left to cure for 20 – 22 hours. Thereafter, the coated gage installation area was covered with a waterproof film before deployment of the gage for CTE measurements in cryogenic cooling tests. A similar procedure was used for a 174 mm long by 25.4 mm diameter Invar 36 cylindrical specimen used as reference material in the CTE testing. The gage type employed was WK series gage, WK-00-250AF-350/W (*VPG*, USA), connected to a portable USB-powered Model D4 data acquisition conditioner (*VPG*, USA) via an RJ-45 connector. The gage has matrix length and width of 14.5 mm and 9.1 mm, respectively. It has a resistance of 350 Ω and a gage factor of 2.00 at ambient temperature. Three gages were used for each concrete mixture. These were bonded to the upper, middle and lower portions on different sides of the concrete specimens.

2.3 Cooling of concrete specimens

The concrete and invar specimens, on which were bonded strain gages were placed in a *Cincinnati Sub Zero* temperature chamber with internal dimensions, 609 mm x 609 mm x 609 mm. The specimens were cooled from ambient to cryogenic temperatures by liquid nitrogen (LN_2) injection from an attached 110-liter dewar (Figures 1a and 1b). The moisture condition of the concrete mixtures just before cryogenic cooling was determined as 62% and 69% of the saturation moisture content for the limestone and trap rock mixtures, respectively. A ramp rate of 3.3°C/min with soaking at selected temperatures for 65 minutes was employed for the cooling program. The ramp rate chosen was the highest possible cooling rate the temperature chamber can easily accommodate. The selected temperatures were 15°C, -20°C, -55°C, -70°C, -120°C and -180°C, although not all temperatures were used in a given experiment. The soaking time of 65 minutes (except at 15°C, for which 60 minutes was used) was chosen after trials showed that the concrete specimens could attain temperatures close to the set point within the time frame. The AE measurements sought to relate detected microcracking to thermal surface strain measurements; hence, it had fewer soak temperatures.

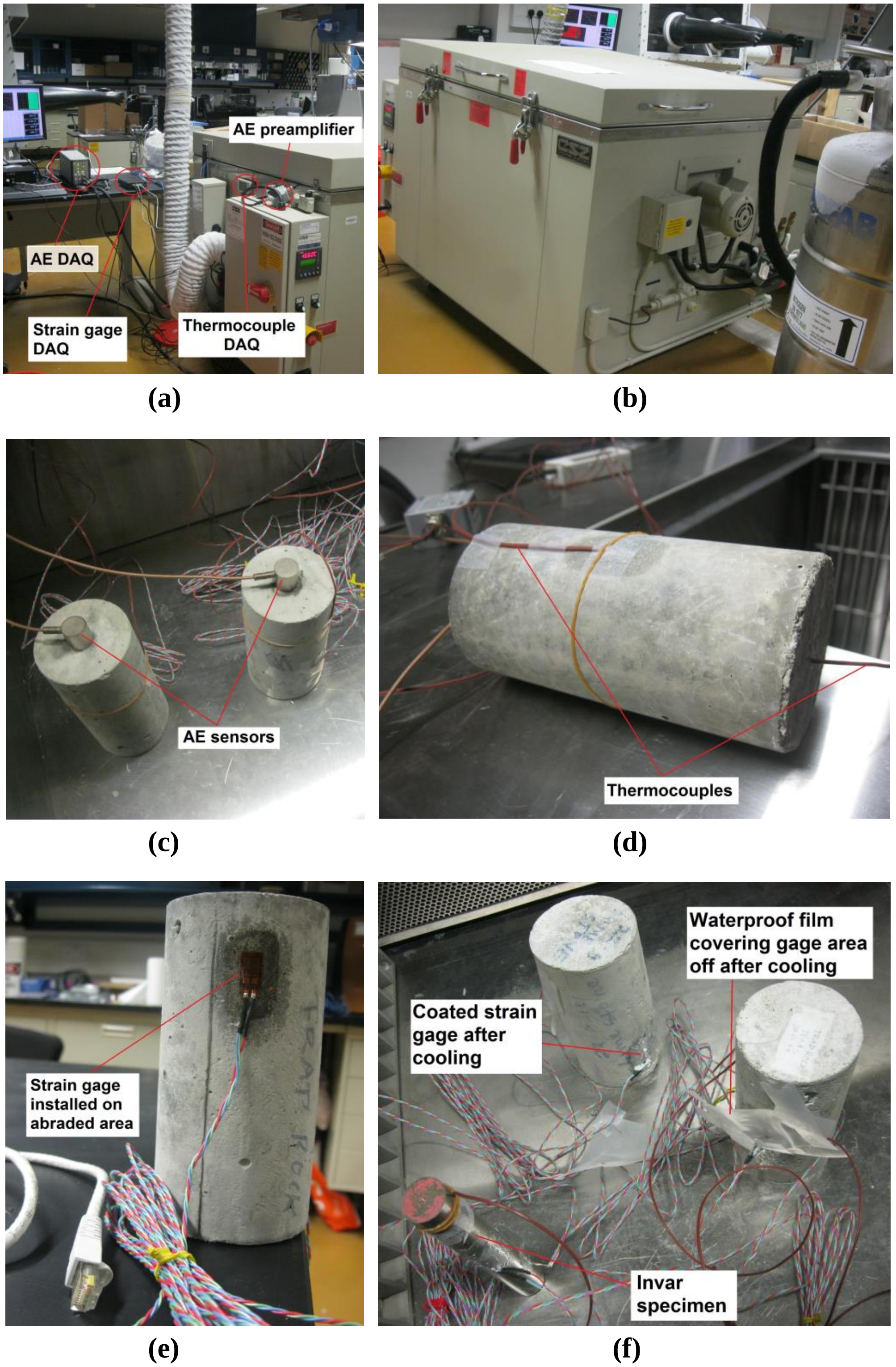

Figure 1. Experimental set-up showing (a) & (b) temperature chamber with data acquisition (DAQ) systems and LN_2 dewar, (c) & (d) AE sensors and thermocouples attachment, and (e) & (f) strain gage installation on concrete and invar specimens.

2.4 AE monitoring of concrete specimens

The AE measurements were carried out on replicates of the specimens used for thermal strain measurements in two separate cooling experiments, one for each concrete mixture. Preliminary testing showed good agreement between replicates in the thermal strain and AE measurements. Pancom 15 sensors (150 kHz resonant frequency) were coupled to abraded areas on the top of two concrete specimens from the different mixtures using a high vacuum sealing compound, HIVAC-G (*Shin Etsu*, Japan) (Figure 1c). The body material of the sensor is nickel-plated brass and the temperature of its detection element (PZT – lead zirconate titanate) can be taken down to -200°C. As opposed to low resonant frequency sensors (60 kHz) commonly used for concrete, the Pancom 15 sensors were used based on availability and from experience that they could perform well in a cryogenic environment. The sensors are specially designed for composite applications. It has been shown that several commercially available sensors with similar characteristics are rugged enough and have sufficient fidelity to be used in a cryogenic environment [9, 16]. The sensors provided AE hits to AEP4 preamplifiers attached to a Vallen AMSY-6 multichannel AE measurement system (*Vallen System GMBH*, Germany), which monitored damage accumulation events during cryogenic cooling. A threshold of 34 dB was used and the sampling rate was 10 MHz. To ensure accuracy of results, the AE data for both concrete mixtures were from the same sensor. In other words, the specimen not from the mixture of interest in a given cooling experiment was used for noise filtering. The detailed procedure for AE data acquisition and post-processing of acquired data is provided elsewhere [8].

2.5 CTE determination from thermal strain measurements

Thermal output (also known as apparent strain) measurements from the strain gages were recorded every 60 seconds during cryogenic cooling. Type T thermocouples placed at abraded surfaces of the concrete and invar specimens, and inserted into the specimens through drilled holes, monitored specimen temperature in parallel with the strain measurements (Figures 1d, 1e and 1f). The CTE was then computed from the thermal output and temperature measurements using Equation 1 [17][1].

$$\alpha_S[\mathrm{T}, \mathrm{T0}] - \alpha_R = \frac{\left(\varepsilon_{TO(S)} - \varepsilon_{TO(R)}\right)}{\Delta T} \quad \textbf{(1)}$$

where α_S is the CTE of the test specimen, α_R is the CTE of the reference material, $\varepsilon_{TO(S)}$ is thermal output on the test specimen, $\varepsilon_{TO(R)}$ is the thermal output on the reference material, and ΔT is temperature change from arbitrary initial reference temperature. The expansion properties of invar from ambient to cryogenic temperatures documented by the National Institute of Standards and Technology (NIST) [18] was used for the reference material.

The CTE computed from the traditional method above was compared with that calculated using the method of algebraic compensation of thermal output strain (TOS) data [19]. This method assumes that the mathematical difference between the known expansion of the reference material at a particular temperature and the TOS at the same temperature is the error that prevents measuring thermal expansion directly. The magnitude of the strain gage error is temperature dependent and is characterized as a function of temperature. It is also independent of the material to which the gage is bonded. The strain gage error is plotted as a continuous curve, over the temperature range, and then curve fit with a polynomial expression. The descriptive equation is then used to compensate TOS data on the test specimen to obtain its thermal expansion [19].

[1] In reality, for a material exhibiting nonlinearity in the thermal deformation response, the CTE should be defined according to $\alpha[T] = \frac{d\varepsilon}{dT}$ such that thermal strain may be expressed by $\varepsilon_{T0(S)}[T, T_0] = \int_{T_0}^{T} \alpha[T] dT$; this form of the constitutive function yields a CTE that is dependent on current temperature but independent of the temperature of the reference configuration. The data in this paper were analyzed using Equation (1) (where CTE is a function of current and reference temperatures) to be consistent with previously published results on thermal response of concrete to cryogenic temperatures.

2.6 Statistics

Pearson and Spearman's rank correlation coefficients were used to measure the degree of association between strain rate and cumulative hits and energy rates, as well as between the strain per unit temperature drop and the cumulative hits and energy per unit temperature. Data pairs for the correlation were taken from any two variables in question during the same or similar ramping or soaking intervals (Appendices A – D). This selectivity was important since the strain and AE tests were done in cooling experiments with some differences in soak temperatures.

The emission rate parameters, cumulative hits and cumulative energy per unit temperature, were computed from the approximate cumulative hits or cumulative energy increment recorded in a given time interval during ramping or soaking, divided by the change in specimen temperature (absolute value) during the interval (Appendices B and D). For instance, in Appendix B, during soaking at 15°C, the cumulative hits per unit temperature (3994) was calculated from the cumulative hits in the interval (10784) divided by the specimen temperature change (18.2°C – 15.5°C) during the interval. Similarly, the cumulative energy per unit temperature (1.67×10^{-10} J/°C) in the same interval was calculated from the cumulative energy in the interval (4.5×10^{-10} J) divided by the afore-stated specimen temperature change (Appendix B, bold row).

3. Results and discussion

3.1 Thermal strain and CTE behavior

The average TOS and specimen temperatures recorded during cryogenic cooling, and the CTEs determined from them are shown in Figure 2a. The TOS was balanced at ambient temperature (22°C) to give a zero strain read out. While the thermal strains derived from algebraic compensation of the TOS and the corresponding CTEs is shown in Figure 2b. The authors are fully aware of the dependence of the CTE on cooling rate, soaking time, etc. Thus, the data in Figure 2 defines the CTE according to the strain at a given time after holding the temperature T, constant at certain ΔT. In other words, the value of the CTE depends on the five selected temperatures and the soaking time at those temperatures. For instance, in calculating the CTE of the specimens at 15°C chamber soak temperature using equation 1, ΔT is taken as the difference between the specimen temperature at 15°C and the initial specimen temperature of 22°C. Similarly, for the CTE at -20°C chamber soak temperature, ΔT is taken as the difference between the specimen temperatures at -20°C and 15°C. Similarly, the ΔT used in calculating the CTE of invar, α_R, which is then used in determining the CTE of concrete (equation 1) was deduced as noted above.

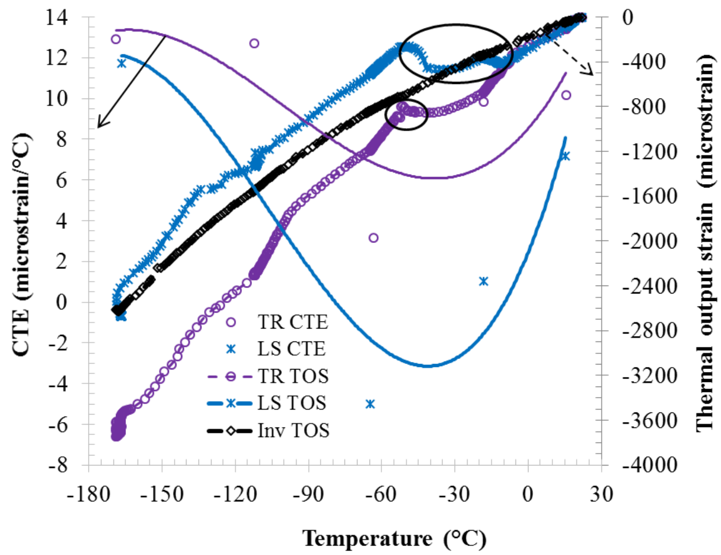

(a)

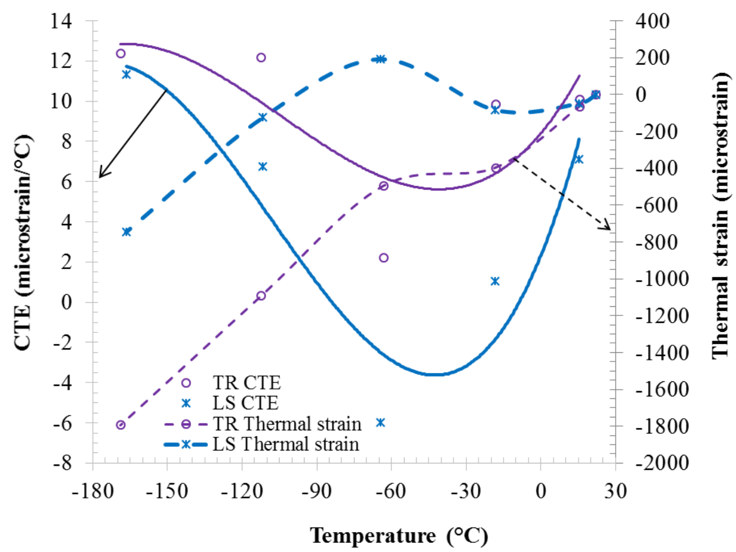

(b)

Figure 2. Thermal (output) strain and CTE of the concrete mixtures during cryogenic cooling, determined by (a) traditional and (b) algebraic compensation methods.

Note: TR: Trap rock concrete, LS: Limestone concrete, Inv: Invar. TOS: Thermal output strain.

The ovals in Fig. 2a indicate the expansion phase during cooling. The arrows with solid line indicates that the fitting curves for CTE is read on the primary (left) vertical axis, while the arrows with dash line indicates that the thermal strain (or TOS) is read on the secondary (right) vertical axis. The ovals and arrows are not part of the data points.

Both methods of CTE calculation resulted in similar CTE values as a single factor ANOVA test of the five data points indicated no significant differences (p-value ~ 0.9) between them. However, the traditional method generally resulted in slightly higher CTE values than the algebraic compensation method. Nevertheless, the latter provides the actual strain unlike the apparent strain in the former. The average CTE over the ambient to cryogenic temperature range is computed as 4.5 μstrain/°C and 9.8 μstrain/°C for the limestone and trap rock mixtures, respectively, using the traditional method. While the algebraic compensation method gives values of 4.1 μstrain/°C and 9.3 μstrain/°C, respectively, for the limestone and trap rock mixtures.

The average CTE of the trap rock mixture is similar to the aforementioned average CTE of 9% Ni or carbon-steel in contrast to the dissimilar CTEs of the limestone mixture and 9% Ni or carbon-steel. In the context of LNG tank design, the trap rock mixture would cause relatively lower tension in the tank bottom plating, thus making it more suitable for direct LNG containment. The thermal strain and CTE behavior of the mixtures is typical of those reported in the literature [1, 2, 5]. The actual thermal strain of the concretes in Figure 2b compares well with the position that cooling from ambient temperature to -165°C can result in contraction of 1500 microstrain [20], albeit this varies with concrete mixtures. The CTE of the limestone (~7 μstrain/°C) and trap rock (~10 μstrain/°C) mixtures near ambient temperature (15°C) are close to values reported in the literature for concrete mixtures employing both aggregates, using different measurement techniques [21, 22]. This is important, as there is a dearth of information in the technical literature on the use of foil strain gages for CTE measurements during cryogenic cooling.

The concrete specimens contracted steadily from ambient temperature to between ~ -10°C and -55°C, where they expanded (Figure 2a). Below -55°C, the concretes resumed contraction down to -165°C. The exact range of the expansion phase in the limestone mixture was -11°C to -52°C, whereas, in the trap rock mixture it was -40°C to -54°C (black ovals in Figure 2a). This agrees with the trend previously mentioned [1, 2, 5, 6] (section 1). However, this work highlights the influence of aggregate type on the temperature range of the expansion phase, in contrast to the position that the amount of expansion and temperature range depends on moisture condition [5]. Especially, as the limestone mixture, which showed greater amount and temperature range of expansion, was at 62% of saturation moisture content compared to 69% for the trap rock mixture before cooling began. The CTE data of the limestone and trap rock mixtures apparently has a turning point around -65°C instead of -55°C due to the choice of temperature points for the CTE determination as there was no soaking at a temperature between -20°C and -70°C.

Noteworthy too, is the occurrence of the expansion phase in wet concretes (not necessarily water-saturated) as most cases of expansion in the literature were linked to water-saturated concretes. The extent of the expansion phase has also been linked to porosity - concrete mixtures with a larger portion of small pores tend to have more pronounced expansion than those with a smaller portion [23]. This is because as the temperature is decreased, the finer pores, which were hitherto filled with super-cooled water, are gradually filled with ice, accompanied by an increase of internal pressure within the aforementioned temperature range(s) [2, 23]. Hence, below the aforementioned temperature range(s) when the finest pores become frozen, the concrete begins contracting again. It was previously shown with nuclear magnetic resonance (NMR) T_2 distribution curves that the limestone mixture apparently had a larger portion of finer pores than the trap rock mixture [9]. This explains the larger expansion range in the limestone mixture than the trap rock mixture. It also probably explains why the CTE of the trap rock mixture did not decrease to negative values like in the limestone mixture during the expansion phase (Figure 2).

3.2 AE behavior and relationship with thermal strain

The AE cumulative hits of both concrete mixtures during cooling are shown in Figure 3. While Figure 4 shows the amplitude, and the absolute and cumulative energies of the mixtures. The specimen temperatures are shown on the secondary axis in the hits and amplitude graphs. The AE tests sought to investigate the microcracking behavior of the concrete specimens at specific temperature regimes during cryogenic cooling. Especially, during the temperature regime (-20°C to -70°C) associated with the expansion phase. Hence, there was no soaking at -120°C for the trap rock mixture (Figure 3a, Appendix B). Similarly, an abortive attempt to obtain the CTE at the extreme of the temperature range of the expansion phase simultaneously with the AE data led to the choice of -55°C instead of -70°C as soak temperature for the limestone mixture. Further, the above rationale for the AE tests led to termination of the cooling of the limestone mixture at -115°C due to limited amount of liquid nitrogen. Especially, as the CTE tests showed linear contraction beyond -70°C (Figure 4b, Appendix D).

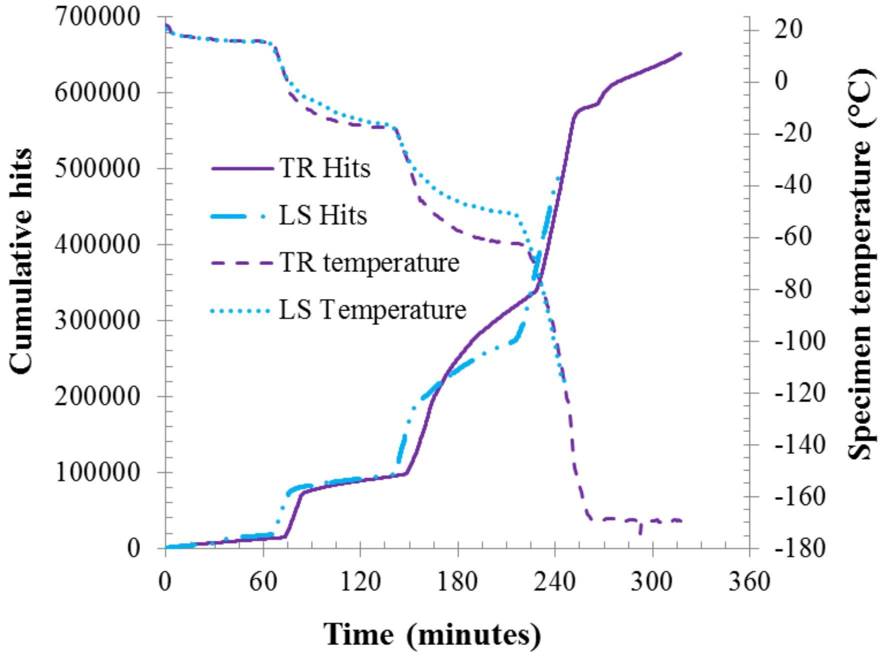

Figure 3. Cumulative AE hits of the trap rock (TR) and limestone (LS) concrete mixtures.

There was initial build-up of medium range amplitude events and significant cumulative energy increase by several orders of magnitude as cooling began (Figures 3 and 4). This could be caused by localized stress from dissimilar volume changes between aggregates and cement matrix arising from temperature change [24]. However, there were very few high amplitude (> 70 dB) events. A few hits with high amplitudes began appearing at specimen temperatures of -15°C and -7°C for the trap rock and limestone mixtures, respectively. High amplitude AE events and steep increases in cumulative hits and energy were initiated as the specimens were cooled below ~ -20°C. Specifically, this occurred at -17°C for the limestone mixture and -25°C for the trap rock mixture. Differences in onset times of high amplitude events in both mixtures may be attributed to differences in pore structure. The limestone mixture has a higher total porosity than the trap rock mixture [9], hence, ice growth tends to occur faster in the former than the latter. Below -20°C, rapid temperature drop during ramping led to large concentrations of high amplitude events, steeper increases in cumulative hits and high increases in energy. The converse occurred during temperature soaking (Figures 3 and 4). The import of this is the influence of cooling rate on microcrack development in concrete. As would be expected, sudden temperature drops lead to significant microcrack development. Conversely, there is little microcrack development with slower temperature changes.

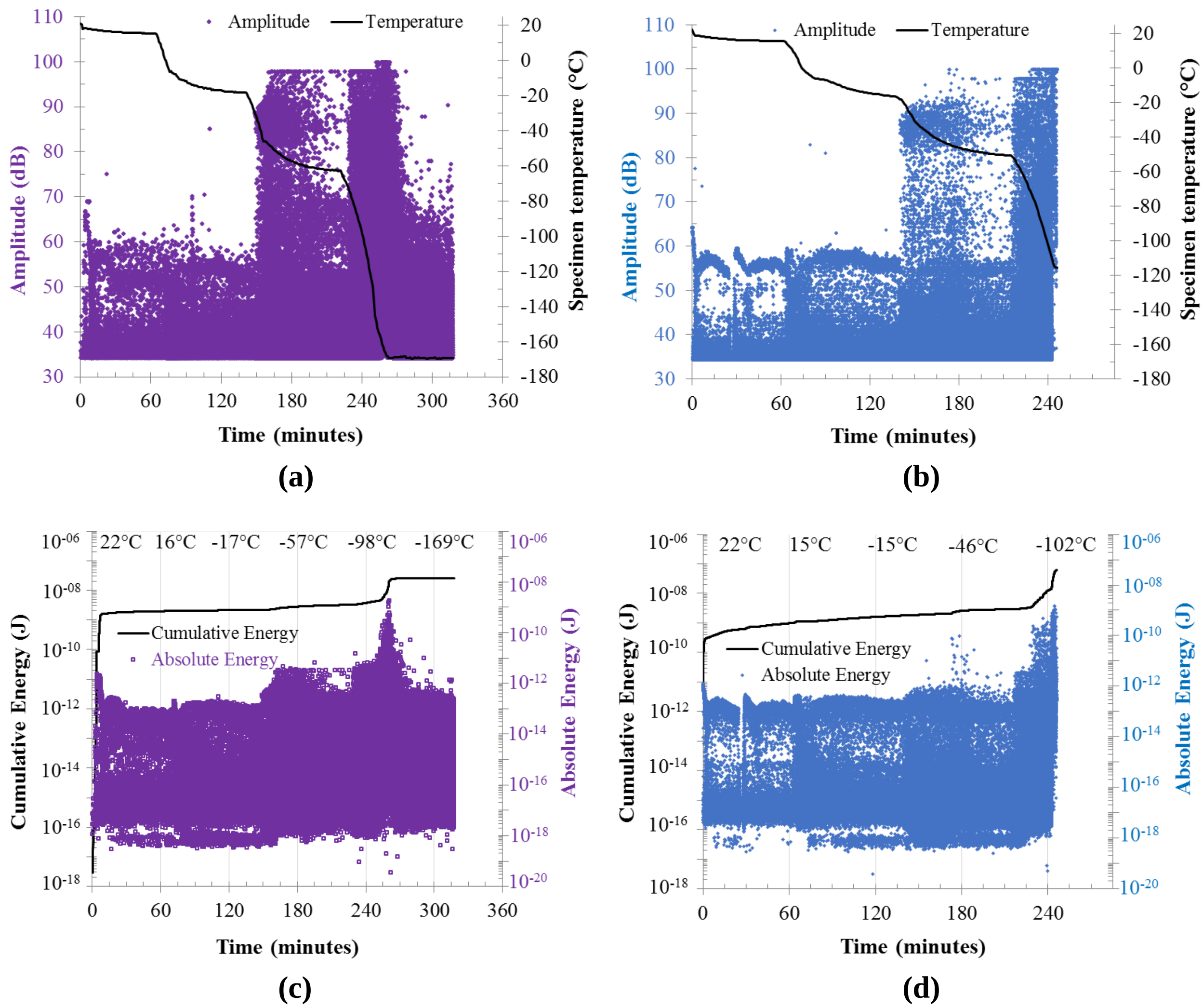

Figure 4. Variation with time during cooling of (a) & (b) AE amplitude and specimen temperature, (c) & (d) AE cumulative and absolute energies, in the trap rock {(a) & (c)} and limestone {(b) & (d)} concrete mixtures.

Note: In Fig. 4a and 4b, the little circular data points for the amplitude are read on the primary (left) vertical axes, while the solid lines for temperature are read on the secondary (right) vertical axes. Similarly, in Fig. 4c and 4d, the solid lines for cumulative energy are read on the primary (left) vertical axes, while the little circular points for the absolute energy are read on the secondary (right) vertical axes. The vertical axes in Fig. 4c and 4d are on a logarithmic scale due to the wide range of the absolute and cumulative energy values.

The AE hits during soaking at -70°C and -55°C in the trap rock and limestone mixtures, respectively, were 3 to 5 times higher than those during soaking at -20°C (Figure 3 and Appendices B and D). This highlights the existence of more microcracking as all pores become filled with ice than at the inception of ice formation. The trap rock mixture had much lower cumulative energy than the limestone mixture, which is indicative of lesser microcracking, although cooling of the latter was terminated with specimen temperature at -115°C compared to -169°C for the former. This could be attributed to greater compatibility of the CTE of the trap rock aggregate with the cement matrix compared to the lower CTE of the limestone aggregate. Generally, the AE trends here are similar to those in previous related publications, which studied different concrete mixtures using the same ramp rate without soaking at specific temperatures. The mechanisms responsible for observed trends were stated in those works [8, 9]. The AE results largely correlate with the thermal strain behavior. The thermal strains are lower at the beginning of cooling with much higher strains as specimen temperatures approach -20°C, similar to the AE results. This is evident in Appendices A and C in which strain levels well above a hundred microstrains were first recorded in the interval during soaking at -20°C for both concrete mixtures. A higher strain level was also recorded during soaking at -70°C than at -20°C, which is in line with the AE results.

Correlations between strain and AE parameters in terms of rates and per unit temperature showed that the strain rate strongly correlated with the hits rate in both mixtures ($p < 0.0006$), but there was no correlation with the energy rate (Figure 5). On one hand, the variation trend with decreasing temperatures of the strain rate is similar to that of the cumulative hits rate. Decreasing temperatures lead to increase in thermal strain and a corresponding increase in cumulative hits due to matrix stresses and microcracking from ice growth. The strain rate and hits rate also follow the same trend during ramping and soaking, as both are higher during ramping than soaking (see Appendices A – D). This explains the strong correlation between the strain rate and the hits rate. On the other hand, the cumulative energy rate and the strain rate do not follow the same variation trend with decreasing temperatures. The cumulative energy rate is quite high at the onset of cooling due to the initial thermal shock in the concrete. It then decreases with temperature to between -20°C and -55°C depending on concrete mixture. The decrease is probably because the hits at this stage are of relatively lower energy as ice begins to form and the concrete 'adapts' to the cooling. Even so, there are increases in strain rate and hits rate as the above temperature range is approached. Thereafter, the energy rate increases with decreasing temperature as cooling progresses beyond the critical temperature regime where expansion occurs due to increase in matrix stresses and microcracking from ice growth (Appendices A – D). Moreover, the strain rate and energy rate follow different trends during ramping and soaking as the energy rate is not necessarily higher during ramping than soaking owing to the above-mentioned behavior. These possibly account for the lack of correlation between both parameters.

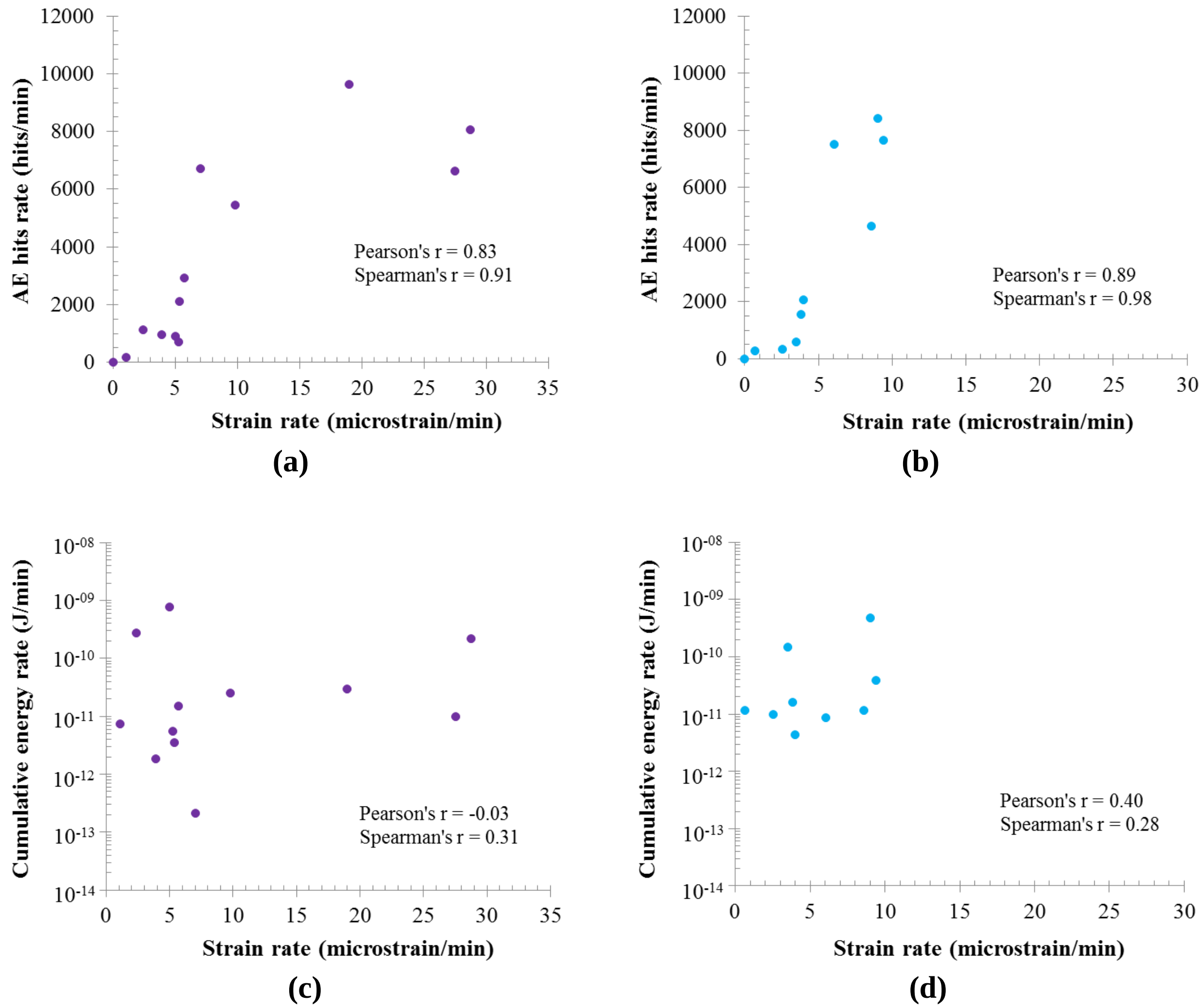

Figure 5. Relationship between strain rates, and cumulative hits and energy rates, during cooling for (a) & (c) trap rock, and (b) & (d) limestone mixtures.

Furthermore, the correlation between the strain, hits, and energy per unit temperature depended on mixture design. The correlation between strain and hits per unit temperature was strong in the trap rock mixture, and moderate but not statistically significant ($p = 0.14$) in the limestone mixture. Similarly, the correlation between the strain and energy per unit temperature was moderate, and weak, in the trap rock and limestone mixtures, respectively (Figure 6). These results show that the cumulative hits rate is a good indicator of thermal strains in the concretes during cooling. There is no clear proportional change in AE cumulative energy with thermal strain in the concretes during cryogenic cooling.

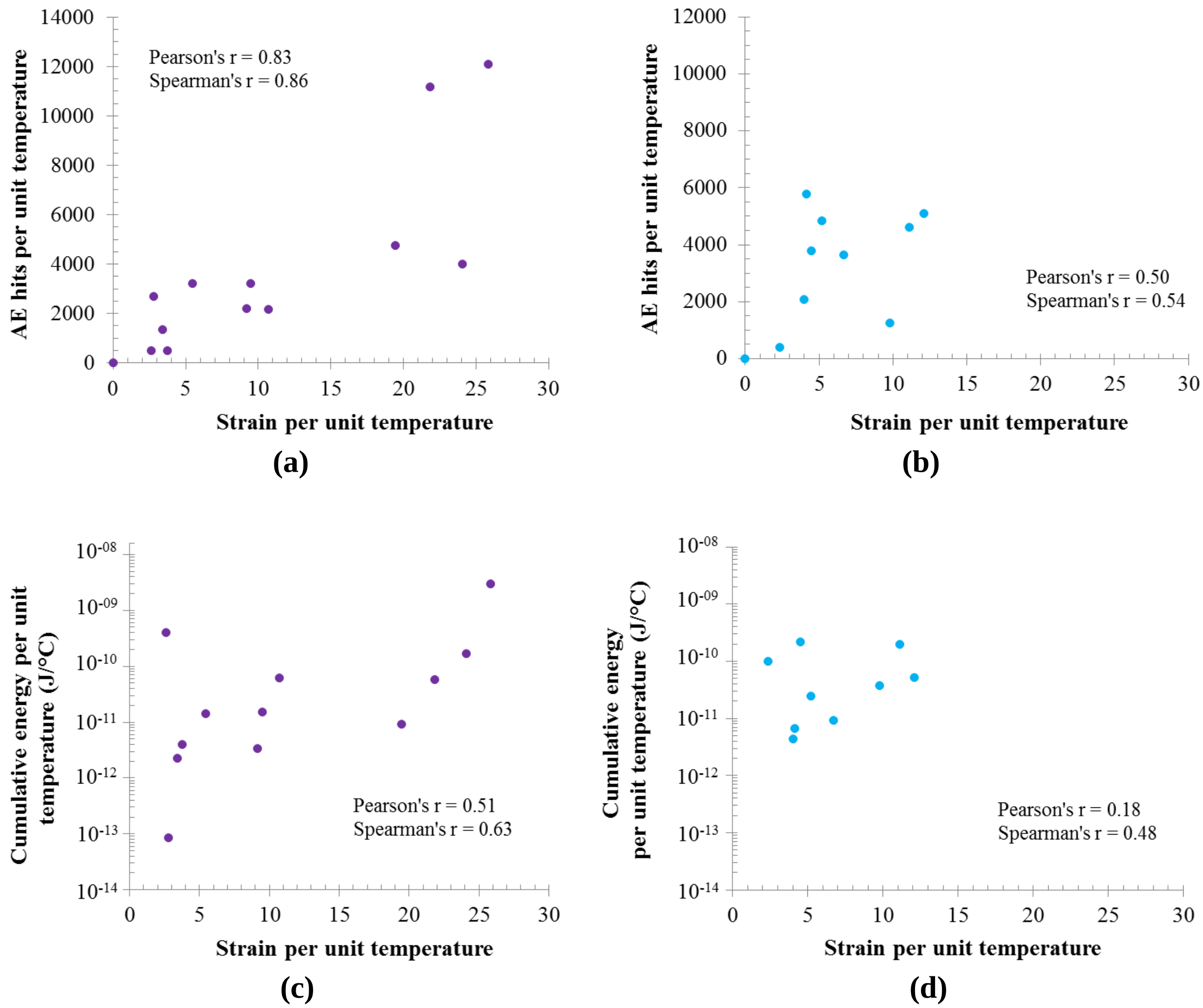

Figure 6. Relationship between strain, and cumulative hits and energy per unit temperature during cooling for (a) & (c) trap rock, and (b) & (d) limestone mixtures.

4. Conclusions

This work has shown that AE provides insight into thermally induced microcracking in concrete and correlates well with thermal strain measurements during cryogenic cooling. The cumulative hits rate strongly correlated with the strain rate in the concrete mixtures studied. Hence, the cumulative hits rate is a good indicator of thermal strains in the concrete mixtures during cryogenic cooling. This contrasts with lack of agreement between both concrete mixtures on clear proportional change in cumulative energy rate, and cumulative hits and energy per unit temperature, with thermal strain. The closeness of the average CTE of the trap rock mixture to that of 9% Ni or carbon-steel, and its lower cumulative energy emission corroborates previous observations on insignificant changes in its porosity, permeability and internal microstructure when subjected to cryogenic cooling. As noted earlier, some other controlling factors such as compressive strength, tensile strength, elastic modulus, etc., are known to improve during cryogenic cooling of concrete. Hence, these observations likely make the trap rock mixture a better choice than the limestone mixture for direct LNG containment.

Acknowledgements

This publication was made possible by an NPRP award (NPRP No. 4-410-2-156: Thermal Dilation and Internal Damage of Cryogenic Concrete Utilized for Direct LNG Containment) from the Qatar National Research Fund (QNRF – a member of The Qatar Foundation). The statements made herein are solely the responsibility of the authors. The authors are thankful to Boback Parsaei of Texas A&M University, College Station, USA, for support for the experiments, and Dr. Ziyad Shafik of Texas A&M University at Qatar Electronic Shop for wiring of the strain gages.

Appendix A

See Table A1.

Appendix B

See Table B1.

Appendix C

See Table C1.

Appendix D

See Table D1.

Table A1. Data table for thermal strains for the trap rock mixture used in Figures 4 and 5

Time (min)	Cooling profile for ramping and soaking temperatures	Chamber Temperature (°C)	Specimen Temperature (°C)	Thermal strain in interval (µstrain)	Thermal strain per minute in interval (µstrain/min)	Thermal strain per °C in interval (µstrain/°C)
0	22°C	22	22	0	0	0
2	3.3°C ramp to 15°C	15	18.2	10	5.00	2.63
62	Soak at 15°C	15	15.5	62	1.03	22.96
73	3.3°C ramp to -20°C	-14	0	58	5.27	3.74
75	3.3°C ramp to -20°C	-20	-5	14	7.00	2.80
140	Soak at -20°C	-20	-18	253	3.89	19.46
154	3.3°C ramp to -70°C	-64	-40	75	5.36	3.41
156	3.3°C ramp to -70°C	-70	-46	55	27.50	9.17
221	Soak at -70°C	-70	-63	371	5.71	21.82
236	3.3°C ramp to -120°C	-113	-90	147	9.80	5.44
239	3.3°C ramp to -120°C	-120	-96	57	19.00	9.50
304	Soak at -120°C*	-120	-112	409	6.29	25.56
323	3.3°C ramp to -180°C	-180	-163	546	28.74	10.71
388	Soak at -180°C	-180	-169	155	2.38	25.83

* Strain/min and strain/°C in this interval not paired with data in Appendix B for correlation calculations. Data in the other 13 intervals were paired to those in the corresponding lines in Appendix B.

Note: The intervals used for relating strain and AE parameters in Appendices A – D were based on ramp time to selected *chamber temperatures* and soak time at those temperatures. In addition, data was taken from the interval involved in ramping to selected *specimen temperatures* such as 0°C, -40°C and -90°C identified in the literature as crucial during water freezing and frost damage in concrete.

Table B1. Data table for cumulative hits and energy for the trap rock mixture used in Figures 4 and 5

Time (mins)	Cooling profile for ramping and soaking temperatures	Chamber Temperature (°C)	Specimen Temperature (°C)	Approximate Cumulative hits in interval	Hits / min in interval	Hits / °C in interval	Cumulative energy in interval (J)	Cumulative energy, J/min in interval	Cumulative energy, J /°C in interval
0	22	22	22	0	0	0	0	0	0
2	3.3°C ramp to 15°C	15	18.2	1833	917	482	1.54×10^{-9}	7.71×10^{-10}	4.06×10^{-10}
62	**Soak at 15°C**	**15**	**15.5**	**10784**	**180**	**3994**	**4.50×10^{-10}**	**7.50×10^{-12}**	**1.67×10^{-10}**
73	3.3°C ramp to -20°C	-14	0	7638	694	493	6.14×10^{-11}	5.58×10^{-12}	3.96×10^{-12}
75	3.3°C ramp to -20°C	-20	-5	13428	6714	2686	4.30×10^{-13}	2.15×10^{-13}	8.60×10^{-14}
140	Soak at -20°C	-20	-18	61732	950	4749	1.19×10^{-10}	1.83×10^{-12}	9.17×10^{-12}
154	3.3°C ramp to -70°C	-64	-40	29584	2113	1345	4.90×10^{-11}	3.50×10^{-12}	2.23×10^{-12}
156	3.3°C ramp to -70°C	-70	-46	13260	6630	2210	2.00×10^{-11}	1.00×10^{-11}	3.33×10^{-12}
221	Soak at -70°C	-70	-63	190184	2926	11187	9.70×10^{-10}	1.49×10^{-11}	5.71×10^{-11}
237	3.3°C ramp to -180°C	-118	-90	87032	5440	3223	3.80×10^{-10}	2.53×10^{-11}	1.41×10^{-11}
239	3.3°C ramp to -180°C	-125	-96	19281	9641	3214	9.00×10^{-11}	3.00×10^{-11}	1.50×10^{-11}
258	3.3°C ramp to -180°C	-180	-163	145065	8059	2165	4.12×10^{-9}	2.17×10^{-10}	6.15×10^{-11}
323	Soak at -180°C	-180	-169	72647	1118	12108	1.81×10^{-8}	2.78×10^{-10}	3.02×10^{-9}

Note: Data in all intervals were paired to those in the corresponding lines in Appendix A (except the line with *) for correlation calculations. The bold row refers to data discussed in section 2.6.

Table C1. Data table for thermal strains for the limestone mixture used in Figures 4 and 5

Time (min)	Cooling profile for ramping and soaking temperatures	Chamber Temperature (°C)	Specimen Temperature (°C)	Thermal strain in interval (µstrain)	Thermal strain per minute in interval (µstrain/min)	Thermal strain per °C in interval (µstrain/°C)
0	22	22	22	0	0	0
2	3.3°C ramp to 15°C	15	19	7	3.50	2.33
62	Soak at 15°C	15	15.4	40	0.67	11.11
74	3.3°C ramp to -20°C	-17	0	103	8.58	6.69
75	3.3°C ramp to -20°C	-20	-1	4	4.00	4.00
140	Soak at -20°C	-20	-18	166	2.55	9.76
155	3.3°C ramp to -70°C	-63	-40	91	6.07	4.14
157	3.3°C ramp to -70°C*	-70	-44	187	93.50	46.75
222	Soak at -70°C	-70	-64.5	248	3.82	12.10
236	3.3°C ramp to -120°C	-113	-90	132	9.43	5.18
239	3.3°C ramp to -120°C	-120	-96	27	9.00	4.50
304	Soak at -120°C*	-120	-112	193	2.97	12.06
323	3.3°C ramp to -180°C*	-180	-160	308	16.21	6.42
388	Soak at -180°C*	-180	-167	313	4.82	46.72

* Strain/min and strain/°C in this interval not paired with data in Appendix D for correlation calculations. Data in the other 10 intervals were paired to those in the corresponding lines in Appendix D.

Table D1. Data table for cumulative hits and energy for the limestone mixture used in Figures 4 and 5

Time (mins)	Cooling profile for ramping and soaking temperatures	Chamber Temperature (°C)	Specimen Temperature (°C)	Approximate Cumulative hits in interval	Hits / min in interval	Hits / °C in interval	Cumulative energy in interval (J)	Cumulative energy, J/min in interval	Cumulative energy, J /°C in interval
0	22	22	22	0	0	0	0	0	0
2	3.3°C ramp to 15°C	15	19	1178	589.00	392.67	2.99×10^{-10}	1.50×10^{-10}	9.97×10^{-11}
62	Soak at 15°C	15	15.4	16644	277.40	4623.33	7.01×10^{-10}	1.17×10^{-11}	1.95×10^{-10}
74	3.3°C ramp to -20°C	-17	0	55928	4660.67	3631.69	1.40×10^{-10}	1.17×10^{-11}	9.09×10^{-12}
75	3.3°C ramp to -20°C	-20	-1	2071	2071.00	2071.00	4.30×10^{-12}	4.30×10^{-12}	4.30×10^{-12}
140	Soak at -20°C	-20	-18	21407	329.34	1259.24	6.36×10^{-10}	9.78×10^{-12}	3.74×10^{-11}
150	3.3°C ramp to -55°C	-55	-31	75070	7507.00	5774.62	8.60×10^{-11}	8.60×10^{-12}	6.62×10^{-12}
215	Soak at -55°C	-55	-51	101756	1565.48	5087.80	1.04×10^{-9}	1.61×10^{-11}	5.22×10^{-11}
227	3.3°C ramp to -180°C	-96	-70	91753	7646.08	4829.11	4.60×10^{-10}	3.83×10^{-11}	2.42×10^{-11}
236	3.3°C ramp to -180°C	-126	-90	75671	8407.89	3783.55	4.31×10^{-9}	4.79×10^{-10}	2.16×10^{-10}
246	3.3°C ramp to -180°C	-149	-115	52030	5203.00	2081.20	5.39×10^{-8}	5.39×10^{-9}	2.16×10^{-9}

Note: Data in all intervals were paired to those in the corresponding lines in Appendix C (except lines with *) for correlation calculations. Where ramping and soaking profiles were different, pairing was based on similar profiles or close temperatures. In other words, ramping and soaking intervals at -70°C in Appendix C were paired with the same intervals at -55°C in Appendix D. While ramping intervals at chamber temperatures of -113°C and -120°C in Appendix C were paired with those at chamber temperatures of -96°C and -126°C in Appendix D.

References

[1] Krstulovic-Opara N. Liquefied natural gas storage: Material behavior of concrete at cryogenic temperatures. ACI Mater J. 2007;104:297 – 306.

[2] Kogbara RB, Iyengar SR, Grasley ZC, Masad EA, Zollinger DG. A review of concrete properties at cryogenic temperatures: Towards direct LNG containment. Constr Build Mater. 2013;47:760-70.

[3] Hoyle K, Oliver S, Tsai N, Hjorteset K, Hjorteset K, LaNier M, et al. Composite concrete cryogenic tank (C3T): A precast concrete alternative for LNG storage. The 17th International Conference & Exhibition on Liquefied Natural Gas (LNG 17). Houston, Texas,2013.

[4] ACI. 376-11. Code requirements for design and construction of concrete structures for the containment of refrigerated liquefied gases and commentary. An ACI Standard. Farmington Hills, MI: American Concrete Institute; 2011.

[5] Marshall AL. Cryogenic concrete. Cryogenics. 1982;November:555 – 65.

[6] Rostasy FS, Wiedemann G. Stress-strain-behavior of concrete at extremely low temperature. Cem Concr Res. 1980;10:565 – 72.

[7] Reinhardt HW. Mechanische en Fysische Eigenschappen van Beton Tussen –190°C en +400°C. Cement. 1979;31:7 - 13.

[8] Kogbara RB, Iyengar SR, Grasley ZC, Rahman S, Masad EA, Zollinger DG. Relating damage evolution of concrete cooled to cryogenic temperatures to permeability. Cryogenics. 2014;64:21 - 8.

[9] Kogbara RB, Iyengar SR, Grasley ZC, Masad EA, Zollinger DG. Non-destructive evaluation of concrete mixtures for direct LNG containment. Mater Des. 2015;82:260 - 72.

[10] De Santis S, Tomor AK. Laboratory and field studies on the use of acoustic emission for masonry bridges. NDT&E Int. 2013;55:64-74.

[11] Flament C, Salvia M, Berthel B, Crosland G. Local strain and damage measurements on a composite with digital image correlation and acoustic emission. 7th European Workshop on Structural Health Monitoring. La Cité, Nantes, France,2014. p. 679 - 85.

[12] Hjorteset K, Wernli M, LaNier MW, Hoyle KA, Oliver WH. Development of large-scale precast, prestressed concrete liquefied natural gas storage tanks. PCI J. 2013;58:40 - 54.

[13] ArcelorMittal. 9% nickel steel: For use at cryogenic temperatures. Product Brochure, ArcelorMittal, USA. Available: http://www.arcelormittalna.com/plateinformation/documents/en/Inlandflats/ProductBrochure/ARCELORMITTAL%209%20PERCENT%20NICKEL.pdf. Accessed March 2015. 2010.

[14] Cross NO, Loushin LL, Thompson JL. Acoustic emission testing of pressure vessels for petroleum refineries and chemical plants. In: Liptai RG, Harris DO, Tatro CA, editors. Acoustic emission, ASTM Selected Technical Papers 505, American Society for Testing and Materials, DOI: 101520/STP35393S1972. p. 270 - 96.

[15] ASTM. C39/C39M-14a - Standard test method for compressive strength of cylindrical concrete specimens. West Conshohocken, PA: ASTM International. doi: 10.1520/C0039_C0039M-14A; 2014.

[16] Walker JL, Workman GL. Study acoustic emissions from composites. Draft Final Report submitted to the National Aeronautics and Space Administration, Marshall Space Flight Center, Alabama. Available: https://ia800501.us.archive.org/30/items/nasa_techdoc_19980048926/19980048926.pdf, [Accessed August 2015]. 1997.

[17] VPG. Measurement of thermal expansion coefficient using strain gages. Tech Note TN-513-1, Vishay Precision Group, Wendell, NC. Available: http://www.vishaypg.com/docs/11063/tn5131tn.pdf, Acessed March 2015. 2010.

[18] Mann D. LNG materials and fluids. First ed: National Bureau of Standards, Cryogenics Division; 1977.

[19] Walsh RP. Use of strain gages for low temperature thermal expansion measurements. In: Haruyama T, Mitsui T, Yamafuji K, editors. Proceedings of the Sixteenth International Cryogenic Engineering Conference / International Cryogenic Materials Conference. Oxford: Elsevier Science; 1997. p. 661-4.

[20] Bamforth PB. The structural permeability of concrete at cryogenic temperatures [PhD Thesis]. UK: Aston University, Available: http://eprints.aston.ac.uk/14275/, [Accessed July 2012]; 1987.

[21] Buch N, Jahangirnejad S. Quantifying coefficient of thermal expansion values of typical hydraulic cement concrete paving mixtures. Final report submitted to The Michigan Department of Transportation, Lansing, MI. Available: https://www.michigan.gov/documents/mdot/MDOT_Research_Report_RC1503_228603_7.pdf. Accesed February 2015. 2008.

[22] Hall KD, James M. PCC materials input values for mechanistic-empirical pavement design guide. Final report (TRC - 0708), University of Arkansas, Fayetteville. Available: http://www.arkansastrc.com/TRC%20REPORTS/TRC%200708.pdf. 2009.

[23] Rostasy FS, Schneider U, Wiedemann G. Behavior of mortar and concrete at extremely low temperatures. Cem Concr Res. 1979;9:365 – 76.

[24] Pour-Ghaz M, Weiss J. Quantifying damage due to aggregate expansion in cement matrix. Advances in the Material Science of Concrete, ACI Special Publication-270-9,2010. p. 101 - 13, doi: 10.14359/51663742.